Materials Science in Semiconductor Processing 126 (2021) 105653

Contents lists available at ScienceDirect

Materials Science in Semiconductor Processing

journal homepage: http://www.elsevier.com/locate/mssp

New hybrid nanocomposite based on (PVA-Ag-Coumarin) for high sensitive photodiode device

M.A. Attallah [a], T.Y. Elrasasi [a], N.M. Shash [a], M.G. El-Shaarawy [a], F. El-Tantawy [b], A. G. El-Shamy [b,*]

[a] Physics Department, Faculty of Science, Benha University, Benha, Egypt
[b] Physics Department, Faculty of Science, Suez Canal University, Ismailia, Egypt

ARTICLE INFO

Keywords:
Photodiode
Schottky junction
Poly vinyl alcohol
Silver nano-particles
Coumarin dye

ABSTRACT

A Schottky device with structure (Ag/PVA-Ag-Coumarin/n-Si) has been fabricated for optical photodiode applications. It has been fabricated via a spin coating technique after preparing PVA-Ag nano-composite using the in-situ technique and then adding Coumarin dye. The photodiode device has displayed good rectification behavior proving the creation of Schottky junction. The high value of the junction parameters, e.g. series resistance $R_{se} = 15$ kΩ, ideality factor $n = 1.463$, as well as height barrier $\phi = 0.779$ eV are calculated from the forward bias I–V characteristics at 50 mW/cm^2 due to the interfaces between the fillers and PVA, creation of barrier height at the interfaces between fillers and PVA, inhomogeneity of the barrier of an interfacial layer of PVA, fabrication and surface processes. Interestingly, Ag/PVA-Ag-Coumarin/n-Si photodiode shows a rise time of 90.2 ms and fall time of 340.6 ms at 50 mW/cm^2. Also, C–V behavior suggested that the device significantly relies on voltage and frequency. The significant increase in the capacitance in lower frequency and the existence of a distinctive peak in the capacitance–frequency behavior refer to interface states. Thus, Ag/PVA-Ag-Coumarin/n-Si devices with their high light sensitivity, are brilliantly applicable in capacitance and/or photodiode sensors for many advantageous uses in modern optoelectronic and electronic industries.

1. Introduction

Recently, optoelectronic materials with high electronic and optical properties are very important for many applications such as p-n junction photodiode and Schottky photodiodes. Photodiode devices have been considered as one of the multipurpose semiconductor electronic apparatuses that convert photon energy into electrical one. Indeed, to detect the wide-range of light (UV, Vis, and IR) spectra, photodiodes are applied. They have a depletion layer with a large electric field that operates on the separation of electron-hole pairs generated by photon/light. To obviate the recombination of electron-holes, these holes and electrons must move in distinct directions. The separation of charge is frequently motivated by a variance in potential at an interface in the semiconductor [1–6]. The photodiodes are characterized by many parameters like series resistance (R_{se}), ideality factor (n), and barrier height (ϕ). The R_{se} is one of the most significant parameters of a diode, which makes the electrical features of the Schottky barrier diodes to be non-ideal [7,8]. I–V features significantly deviate from the linear behavior particularly at high forward bias region when a diode has an adequate large R_{se} value (a few Ω). Research on photodiode devices at the outset was performed using classic inorganic materials such as ZnO, Mg, Al, and others due to their boosted photo-responses. However, these inorganic substances have shown significant deficiencies as their high costly raw materials, harmfulness, plus their limited abundance [9]. Besides, their complicated preparation methods, which raise the cost. Thus, it is hard to insert these materials into devices and also it is not easy to recycle them. Furthermore, they have weak mechanical properties, which make them incompatible for the development of bendable devices [10]. Thus, it is necessary to develop flexible, economical, environmentally friendly, lightweight, and highly-performing materials. Thus, recent substances based on dye-polymeric nano-composites with high photo-response were developed for photodiodes. Many literatures have been reported based on the role played by polymeric nano-composites in improving photodiode performance and quality. For example, ZnO/PVA/graphene quantum dot nanocomposite system has been designed to increase the response of the photodiode [11]. Also, the

* Corresponding author.
E-mail address: agabedelazim@yahoo.com (A.G. El-Shamy).

https://doi.org/10.1016/j.mssp.2020.105653
Received 24 November 2020; Received in revised form 22 December 2020; Accepted 28 December 2020
Available online 11 January 2021
1369-8001/

photodiode device has been manufactured based on Au/PVA (Bi-doped)/n-Si to improve the photodiode parameters [12]. In fact, among all the polymers, PVA is a unique polymeric material due to its easy preparation, durability, chemical resistance, thermostability, high mechanical properties, and its dielectric properties [13]. Besides, PVA has been extensively used in the field of nanotechnology as a reducing and stabilizing agent in the fabrication of nanoparticles [14]. Moreover, silver as a conducting particle was embedded in different crystalline, amorphous and polymeric materials to improve their electrical, mechanical, and other properties [15,16]. On the other hand, Coumarin has attracted great interest when compared with all dyes [17]. Coumarin dye is composed of two rings linked with each other. These rings are lactone and benzene. These two rings have either a double bond structure or a conjugated π-system. It is worth to mention that, this conjugated π-system facilitates the electron exchange between PVA and coumarin. The obtained structure remains scarce to maintain mechanical flexibility. It is predicted that the barrier height increases, due to the influence of coumarin on the space-charge region of the Schottky junction. The electronic features of coumarin have been investigated broadly and it was found that the time of reaction raises as well as the resistivity decreases in general [18]. A large amount of works on enhancing the photodiode performance has been reported, however, the door is still open for developing the photodiode parameters to fulfill the desires. So, we introduce a new Schottky device based on PVA-Ag-Coumarin dye films for photodiode applications.

The present investigation is devoted to fabricate a new Ag/PVA-Ag-Coumarin/n-Si photodiode. In fact, among all polymers, polyvinyl alcohol (PVA) is selected in this work to make thin interfacial layers that produce an interface charges with bias, thanks to the extra electric fields in the interfacial layers and their effects on the electrical behavior of the diode particularly under illumination conditions. Also, the selection of silver (Ag) nanoparticles is due to its high optical, electrical, and high optoelectronic properties which help in increasing the electrical behavior of the diode. Also, coumarin dye is chosen due to (i) its conjugated π-system facilitates the electron exchanges between PVA and coumarin and (ii) its higher response to the UV light which may be useful in the charge transfer complex system in the nano-composite. In this work, the in-situ method was applied to obtain the reduction for Ag^{+} to Ag nanoparticles through the activation of (-OH) of PVA, after that different concentrations of Coumarin dye were added to PVA-Ag solution to produce the PVA-Ag-Coumarin nanocomposite films. The spin coating method has been applied to engineer the Schottky diode for photodiode application. The average size of Ag nanoparticles inside the matrix was found to be 40.2 ± 5 nm. The photodiode device exhibited good rectification behavior with a rectification ratio of 3.7 at applied voltage = ±4 V, proving the creation of Schottky junction. The ideality factor n = 1.463, series resistance R_{se} = 15 kΩ and the height barrier ϕ = 0.779 eV were calculated from the forward bias I–V characterstics at 50 mW/cm^2 due to the interfaces between the fillers and PVA, creation of barrier height at the interfaces between fillers, PVA inhomogeneity of the barrier of an interfacial layer of PVA, fabrication and surface processes. Interestingly, Ag/PVA-Ag-Coumarin/n-Si photodiode shows a rise time of 90.2 ms and fall time of 340.6 ms at 50 mW/cm^2. More excitingly, the diode displays current in the forward and reverse bias under the illumination conditions. Also, C–V behavior suggested that the device significantly relies on voltage and frequency. The significant increase in the capacitance in lower frequency and the existence of a distinctive peak in the capacitance–frequency behavior refers to the possession of interface states. Thus, Ag/PVA-Ag-Coumarin/n-Si devices show a high light sensitivity, giving them the merit to be brilliant applicants as capacitance and/or photodiode sensors for optoelectronic applications in the modern electronic industry.

2. Experiments and methods

2.1. Materials

Polyvinyl alcohol $[CH_2CH(OH)]_n$ (99.8% purity), silver nitrate ($AgNO_3$, 99% purity), HF acid, and Coumarin ($C_9H_5O_2$) have been brought from the Alfa Aesar Chemicals.

2.2. Fabrication of nano-composite PVA-Ag films

Nano-composite PVA-Ag films have been designed by in situ chemical reduction approaches under a hot condition supported by the solution casting techniques as follow [19–21]: a solution of PVA has been prepared by resolving 0.75 g of PVA in 25 ml deionized water with continues stirring at 70 °C for 2 h even the mixture was fully solved. Then, freshly $AgNO_3$ solution, which is prepared by dissolving 0.3 g/30 ml deionized water at ambient temperature with continuous stirring for 20 min, was added up to the solution of PVA under a hot condition (60–70 °C) and the reaction was kept for 1 h to reduce the silver nitrate to silver nanoparticles by the (-OH group) in PVA [22–24].

2.3. Synthesis of PVA-Ag-Coumarin nano-composite films

After obtaining (PVA-Ag) nano-composite, Coumarin dye solution, which is prepared by dissolving 0.8 g/400 ml deionized water for 1 h at ambient temperature, was added to the above mixture (PVA-Ag). Then, the mixture was left for about 24 h at ambient temperature to verify a homogenous and air bubble-free solution, which was casted in the glass dish to obtain the films.

2.4. Fabrication of Ag/PVA-Ag-coumarin/n-Si photodiode

The spin coating technique was applied to prepare Ag/PVA-Ag-Coumarin/n-Si photodiode (Scheme 1). At first, HF acid was conducted to remove both deionized water and the native oxide layer on the silicon wafer before the fabrication of the device. Then, the silicon wafer was immersed in successive baths of acetone and methanol [25]. Immediately after cleaning the surface, silver (Ag) with a 150 nm thickness was coated onto the whole back surface of the n-Si wafer to obtain an ohmic contact. Ohmicity of the contact was controlled by I–V measurements and the contact has shown a good ohmic behavior. After the n-Si wafer is ready for the coating process, the nano-composite was coated on the surface of the n-Si wafer with (5000 rpm) then left to air-dry. After that, Ag electrodes were made onto PVA-Ag-Coumarin film and the n-Si wafer. 200 nm was the thickness of the film by AFM. The contact area of the diodes was determined to be 3.51 × 10^{-2} cm^2.

2.5. Measurements

X-ray diffraction (XRD) patterns of the nano-composites have been detected by X-ray –D/Max 2200V-Rigaku-Japan diffractometer with a monochromatic beam of wavelength 0.154 nm Cu Kα radiation from 5° to 80°. TEM microscope, with a Model: (JEOL-JEM-1230) works at 100–120 kV, has been used to detect the average size of Ag particles and their standard deviation by taking a drop from the redissolved film into a carbon-coated copper grid. The optical absorption spectra were measured by JANEWAY 6405 UV/VIS spectrophotometer as a function of wavelength λ (nm) in the range from 200 to 800 nm. A Quanta 250 FEG SEM microscope was applied to study the surface morphology of the samples using an electron beam with a current of 40 nA and energy 15 keV. The atomic force microscopy (Bruker. Model:- MLCT-MT-A) was used to evaluate the thickness of the coated films. Keithley 4200 semiconductor system was conducted to measure the I–V diode features in the illumination intensity range of 10–50 mW/cm^2 and dark conditions. 150 W halogen lamp has been used as a white light emitted source. PM 6304 programmable automatic RLC meter was also applied to study the

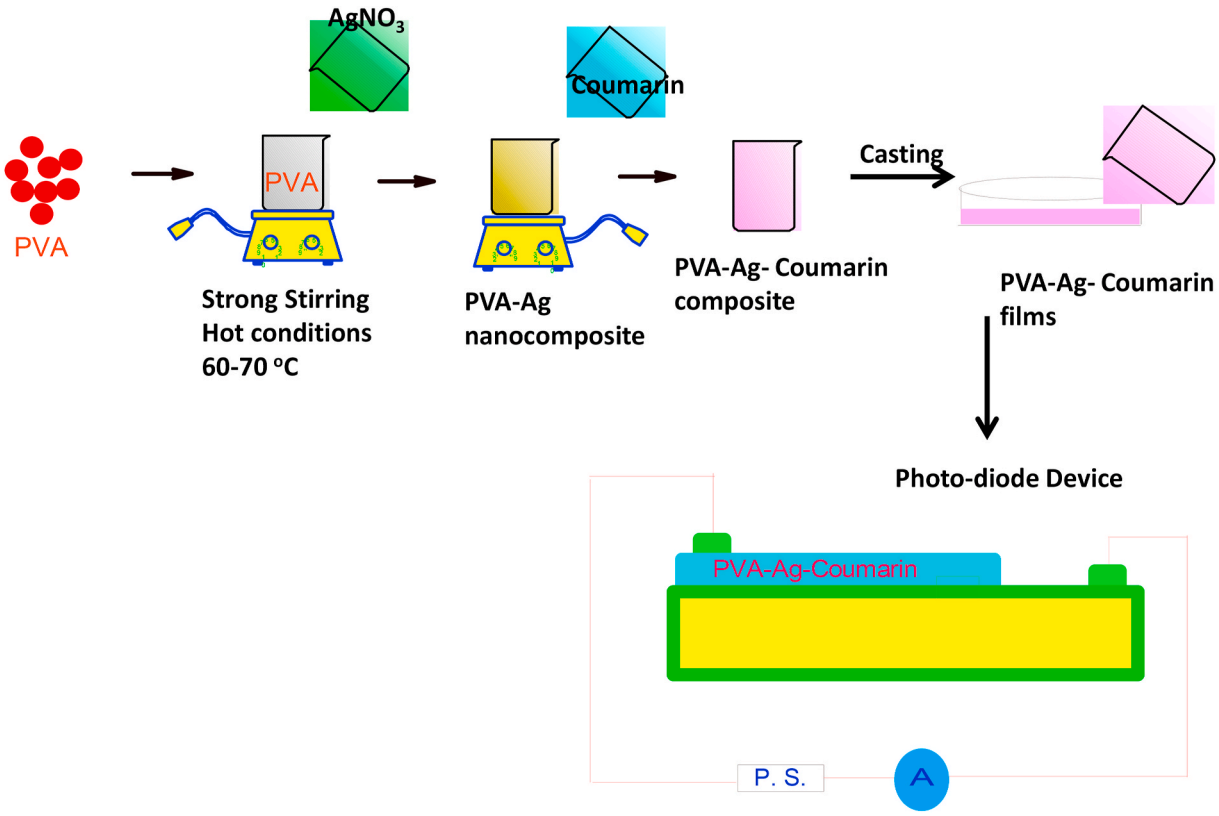

Scheme 1. Shows the steps of preparation and fabrication of the PVA-Ag-Coumarin nanocomposite films and its Schottky diode.

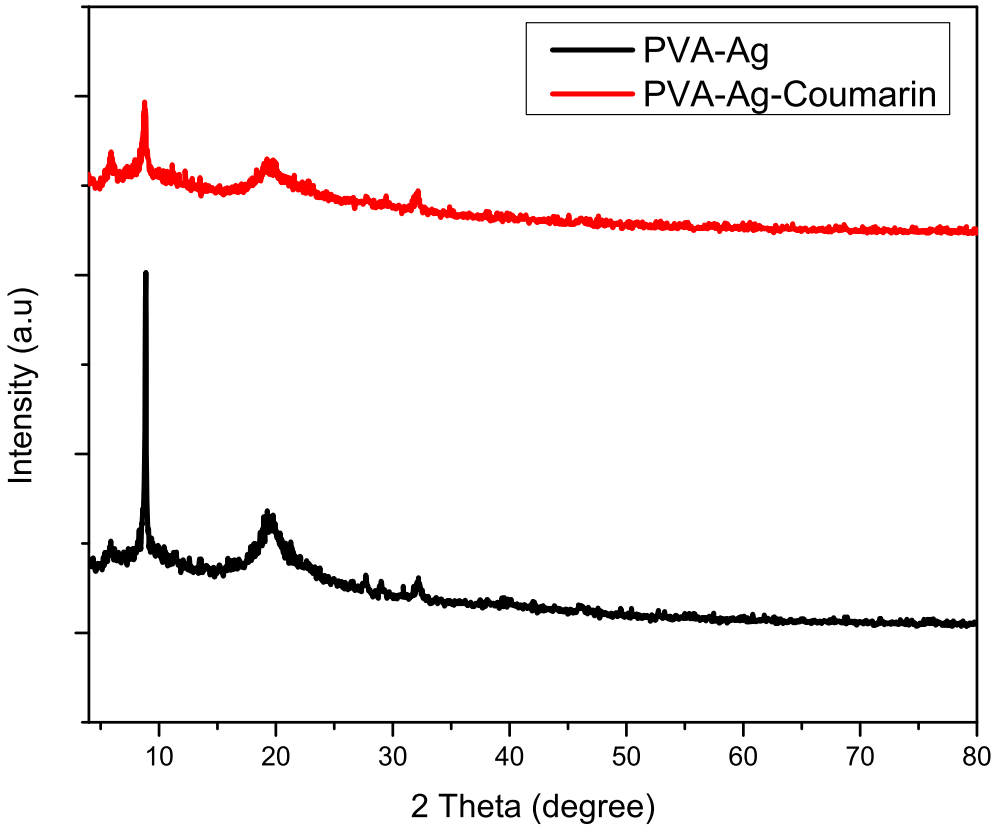

Fig. 1. Shows the XRD patterns of PVA-Ag and PVA-Ag-Coumarin dye nanocomposite films.

capacitance voltage (C–V) of the diode.

3. Results and discussions

3.1. Structural & morphological properties of the films

XRD patterns of PVA-Ag and PVA-Ag-Coumarin nano-composites are shown in Fig. 1. The main peak can be seen at $2\theta = 19.9^{\circ}$ for the two samples, which represent the crystalline region of the semi-crystalline PVA polymer [26]. The intensity of this peak is decreased by adding the Coumarin dye which refers to the decrease in the crystallinity of the nano-composite films. The crystallinity of the nano-composites was calculated from the ratio between the integrated area under the crystalline parts and the integrated area under the whole XRD chart [27] and it was found to be 47.2% for PVA-Ag and 44.4% for PVA-Ag-Coumarin. This decrease in the crystallinity was attributed to the strong interaction between Coumarin and PVA-Ag composite which leads to an increase in the disordering behavior inside the nano-composite [28–30]. Beside this peak, a strong peak was observed at $2\theta = 9.8^{\circ}$, this peak neither belongs to $AgNO_3$ nor pure PVA crystalline spectra, but it possibly arises from scattering the atomic plane of some crystalline patterns of PVA-Ag^{+} complex [31,32]. Also, the intensity of this peak decreases with coumarin dye content, which reveals strong interaction between PVA-Ag nano-composite and coumarin dye and proves the role of Coumarin in destroying the crystalline planes and increasing the amorphous regions in the nano-composite. This means that Coumarin dye has a strong effect on controlling the reaction, i.e coumarin may accelerate the reaction between PVA and Ag. However, no peaks appeared for Ag nanoparticles, this is probably due to the tiny Ag nanoparticle size formed in the nano-composite. Similar behavior was observed in the literature [22]. To confirm the formation of Ag nanoparticles, TEM image was carried out (Fig. 2). As seen, TEM image shows that Ag is present in the nanoscale and its average size is 40.2 ± 5 nm. Ag nanoparticles have a spherical shape with uniform edges. Also, the strong adhesion of PVA polymers on the surface of Ag was observed proving the strong interaction between PVA and Ag with the presence of Coumarin.

On the other hand, SEM and EDX analyses for the surface of the films were performed to study the surface morphology and identify the elements in the nano-composite. Fig. 3 shows SEM image and EDX spectra of PVA-Ag and PVA-Ag-Coumarin nano-composite. As seen, Ag nanoparticles were arranged uniformly with a spherical shape. Also, they are segregated from the matrix of PVA by adding Coumarin. This behavior leads to creating a conductive path of Ag nanoparticles and improving the particle-particles behavior and hence increasing the conductivity. EDX spectrum confirms the subsistence of perfect quantities of silver in PVA host matrix. As seen, three elements were detected at energies 0.2, 0.5 and 3.2 KeV for the C, O, and Ag, which are the content of the nano-composite.

3.2. Optical properties of the films

Fig. 4 shows the optical spectra (absorption, *A*) for the PVA-Ag and PVA-Ag-Coumarin dye nano-composites. As seen, two absorption peaks were detected in the UV region for PVA-Ag film. These peaks were located at $\lambda = 200$ and 275 nm. The peak at $\lambda = 200$ nm appeared due to the n–π* transition for the unsaturated bonds C═O and/or C═C that exist in PVA tail–head. Also, the peak at $\lambda = 275$ nm appeared due to the π–π* transition for the charge transfer group [19–24]. However, in PVA-Ag-Coumarin films, the intensity of these peaks increases due to the addition of Coumarin dye in the composite, which increases the n–π* and π–π* transitions by increasing the number of the unsaturated C═O and/or C═C bonds and charge transfer complex inside the films. However, in the visible regions, a peak at $\lambda = 436$ nm was detected for PVA-Ag composite due to the creation of Ag in the nano-scale. The corresponding reduction of Ag ions in metallic silver $Ag^{+} + e^{-} \rightarrow Ag$ was produced by the activation of (-OH) group of PVA [19–24]. This peak intensity increases in case of PVA-Ag-Coumarin film, owing to the increase in the number of Ag nanoparticles in the matrix. This behavior confirms the role of Coumarin in the reaction and formation of Ag nanoparticles.

The optical bandgap of the nano-composites was determined by the following relation [19–24]:

$$(\alpha h\nu)^{s} = M\left(h\nu - E_g\right) \quad (1)$$

where *M* is constant, E_g is the optical bandgap and *s* is an exponent that depends on the optical transition type.

Fig. 5 shows $(\alpha h\nu)^{0.5}$ vs.$h\nu$for PVA-Ag and PVA-Ag-Coumarin dye nano-composites. The values of the optical bandgaps are evaluated from the linear fitting straight lines as reported in Refs. [19–24]. It was found that the energy bandgap has been decreased from 2.5 eV for PVA-Ag to 2 eV for PVA-Ag-Coumarin. This depression in the optical bandgap value on PVA-Ag with coumarin renders to the induction of a photochemical reaction by the effect of coumarin dye on the nano-composite that inspires more stenography of the residual Ag ions in the metallic silver $Ag + e^{-} \rightarrow Ag$. This happens during the release of an electron from PVA chain, and elevating the metallic silver concentration in the nano-composite. These Ag nanoparticles are in charge of the

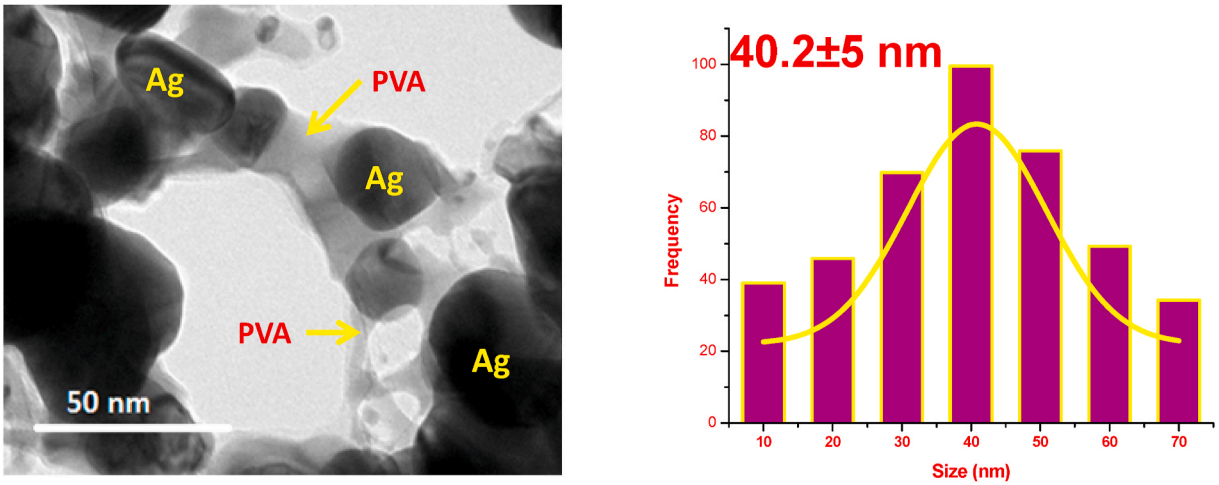

Fig. 2. Shows (a) the TEM image of the PVA-Ag nanocomposite by taking a drop from the re-dissolving of the nanocomposite on a carbon coated copper grid (b) histogram shows the size distribution of the Ag nanoparticles inside the sample.

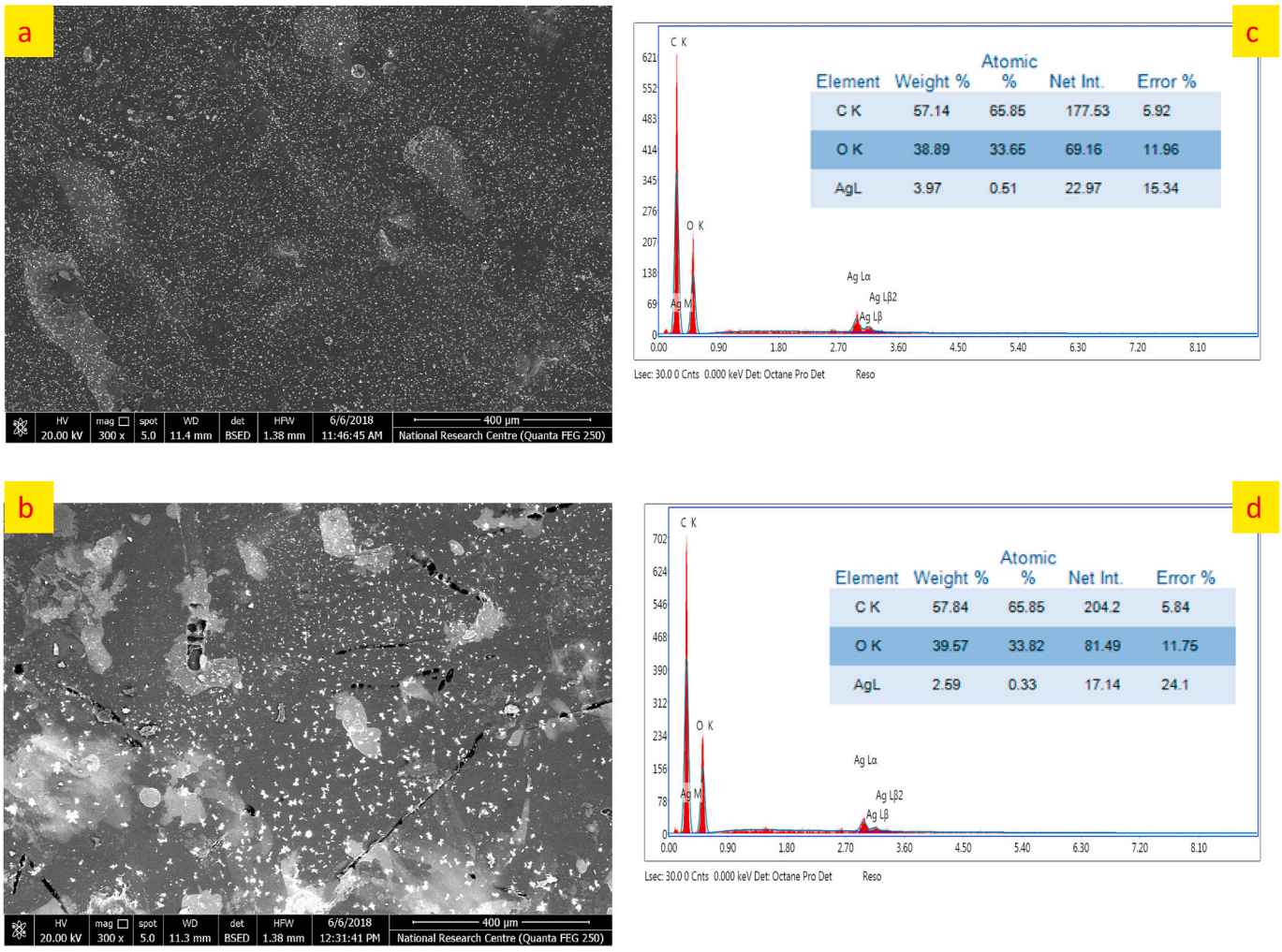

Fig. 3. Shows (a) SEM image of PVA-Ag nanocomposite films (b) SEM image of PVA-Ag-Coumarin nanocomposite films (c) EDX spectra of the PVA-Ag nanocomposite films (d) EDX spectra of PVA-Ag-Coumarin nanocomposite films.

formalization of centralized electronic states in the HOMO and LUMO orbitals. This centralized state acted as a trapping and recombination center, thus, facilitating low energy transitions, producing the noticed modulation in the band gap.

3.3. The diode performance

Fig. 6 clarifies the I–V behavior of Ag/PVA-Ag-Coumarin/n-Si diode under dark and different intensities of illumination. The photodiode displayed a good rectification performance with a rectification ratio of 3.7 at applied voltage = ±4 V. The rectification performance was detected owing to the creation of the Schottky junction at the n-Si substrate and the nano-composite interfaces [33]. Notably, by increasing the intensity of illumination, the diode possesses a current in both the reverse and forward bias. At a certain voltage, the photodiode possesses a higher reverse current under lighting conditions than that in the dark conditions, proving the good rectification behavior. Moreover, non-saturating behavior was observed in the reverse bias I–V characteristics. The image of lowering forces of barrier height can illustrate this non-saturating behavior [33,34] and the presence of PVA layers at nano-composite and Si interfaces. Photons acquire energy (E = hc/eλ) under illumination conditions higher than the energy band gap of the composite that can produce a pair of (e^-/h^+) in the depletion layer at the interface. Subsequently, the structure is stressed with an electrical field, this pair of (e^-/h^+) is isolated/separated under the strong localized electrical fields that are produced internally at the grain boundaries. Holes are slowly removed from PVA layers under the effect of the electrical fields however, the electrons are rapidly removed therefore they could be trapped by the defects.

The Schottky (ideality factor n, series resistance R_{se} and effective barrier height ϕ) parameters are determined from the forward bias I–V characterstics. From the theory of thermionic emission, the Schottky diode can be explained as [35].

$$I = I_o\left[\exp\left(\frac{qV}{nkT}\right) - 1\right] \quad (2)$$

where q is the electronic charge, the ideality factor is donated by n, the Boltzmann constant is donated by k, the applied voltage (V), absolute temperature (T), and the reverse saturation current is donated by I_o and given by [35].

$$I_o = AA^*T^2\exp\left(-\frac{q\phi}{kT}\right) \quad (3)$$

where A is the area of the device, the effective Richardson constant is donated by A^* and the barrier height is donated by ϕ. The ideality factor (n) can be calculated from the ln(I)–V plot of the forward bias by taking the slope of the linear part through the relation [36],

$$n = \frac{q}{kT}\left(\frac{d(V)}{d(\ln I)}\right) \quad (4)$$

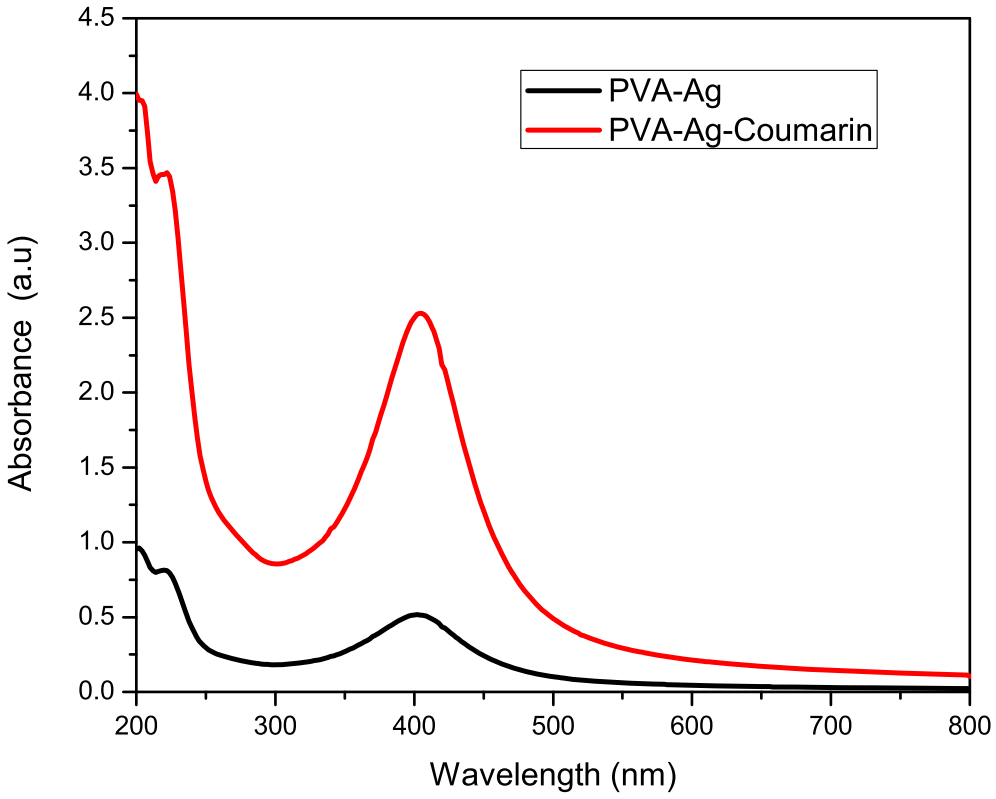

Fig. 4. Shows the optical absorption spectra for the PVA-Ag and PVA-Ag-Coumarin dye nanocomposite films.

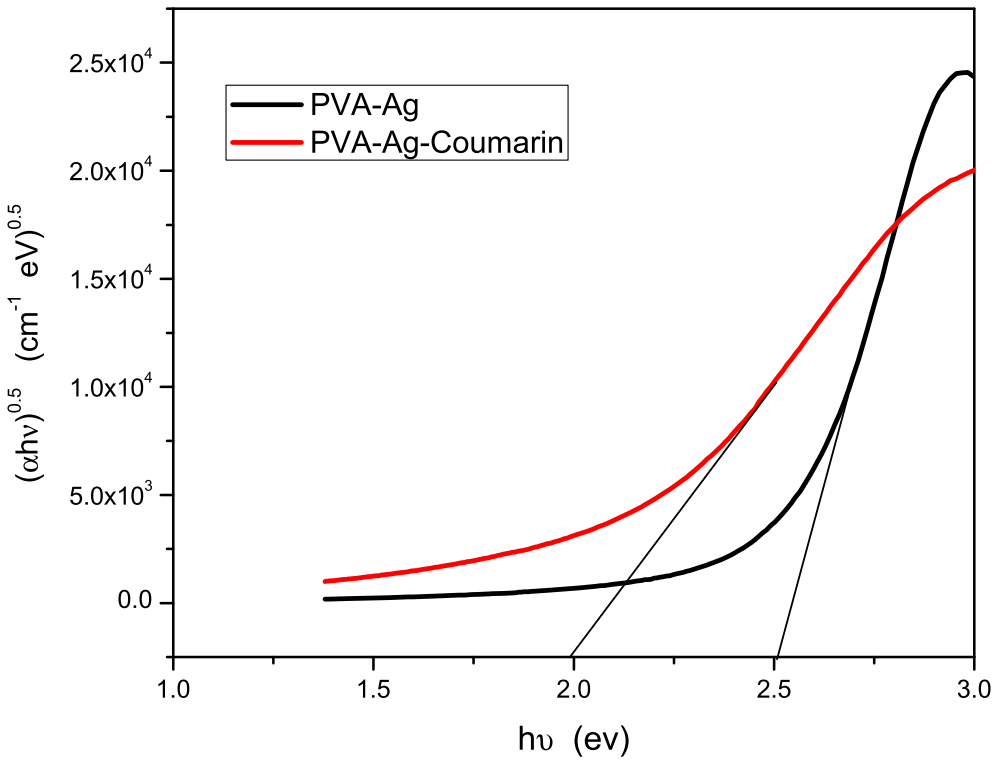

Fig. 5. Shows the band gap of PVA-Ag and PVA-Ag-Coumarin dye nanocomposite films.

The barrier height ϕ has been determined from,

$$\phi = \frac{kT}{q}\ln\left(\frac{AA^{*}T^{2}}{I_o}\right) \quad (5)$$

Fig. 7 shows the semi-logarithmic ln(I)–V of Ag/PVA-Ag-Coumarin/n-Si diode under different intensities of illumination and dark conditions. The diode parameters are listed in Table 1. It is noticed that the reverse saturation current increases by increasing the intensity of

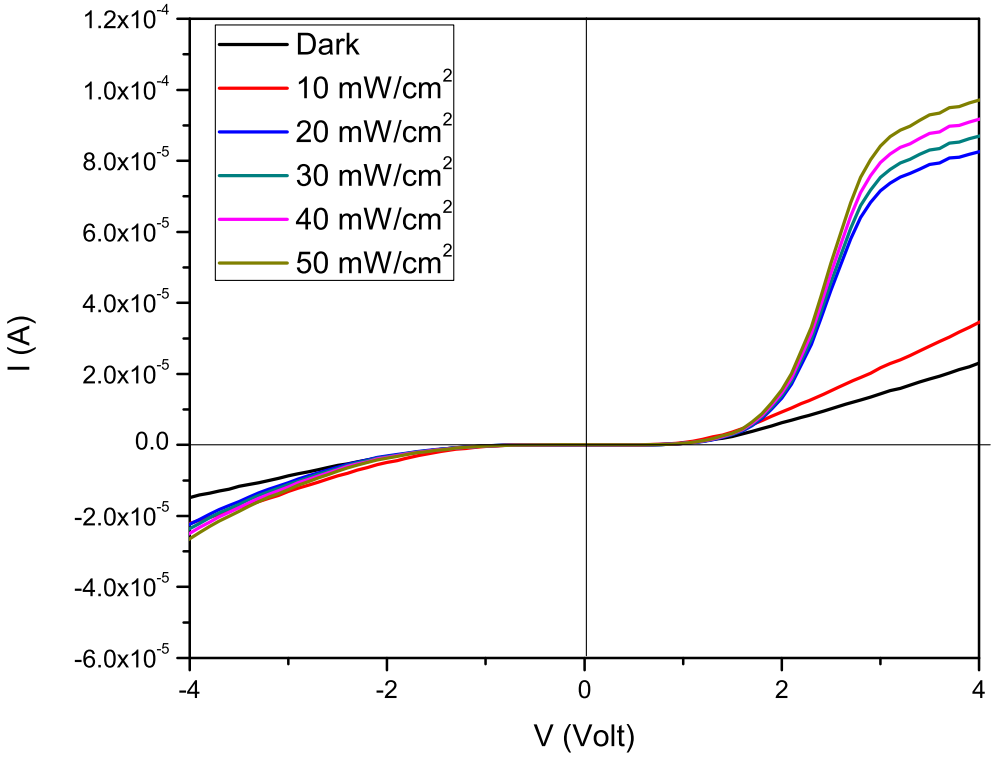

Fig. 6. Shows the I–V characteristics of the Schottky diode under the dark and different intensity of illumination (10–50 mW/cm^2) at room temperature.

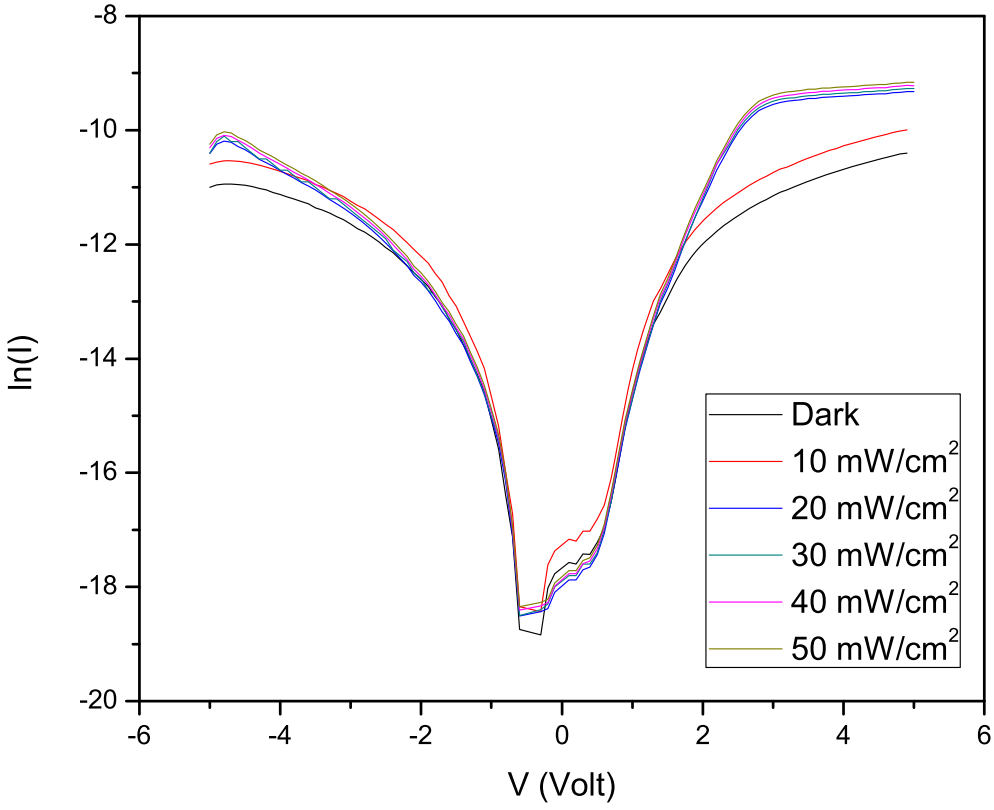

Fig. 7. Shows the ln(I)–V characteristics of the Schottky diode under the dark and different intensity of illumination (10–50 mW/cm^2) at room temperature.

illumination. This increase is possible because of the generation of charge carriers upon the light absorption. An additional current will be produced by these carriers and will flow across the junction, added to the dark current. Ideality factor (n) increases from 1.275 at dark to 1.463 at the intensity of illumination 50 mW/cm^2. This could be due to the recombination of (e^-/h^+) in the depletion layer. In addition to the

Table 1
The ideality factors (n), barrier height (ϕ) and series resistance (R_{se}) at different illumination intensities.

Intensity (mW/cm^2)	Saturation current I_o(A)	Barrier height ϕ (ev)		Ideality factor (n)		series resistance R_{se} (kΩ)	
		I–V	dV/dln(I)	I–V	dV/dln(I)	dV/dln(I)	H(I)
Dark	1.448×10^{-8}	0.782	1.1	1.275	1.9	131	130
10	2.341×10^{-8}	0.769	0.89	1.497	6.35	68	70
20	1.337×10^{-8}	0.784	1.01	1.463	3	26	31
30	1.410×10^{-8}	0.782	0.39	1.463	2.6	33	34
40	1.478×10^{-8}	0.781	0.82	1.463	7.6	10	20
50	1.569×10^{-8}	0.779	0.90	1.463	4.5	15	24

ideality factor (n) values are higher than the ideality factor of ideal semiconductor diode (n = 1). The observed higher ideality factor values are larger than unity denoting the existence of heterogeneities in barrier height. These heterogeneities may be due to many factors: (i) the difference in the work function of Ag contact and n–Si. (ii) pinning of the Fermi level at the interface (iii) image forces acting on barrier height, (iv) tunneling current, and (v) the formation of interface states as well as the existence of series resistance [37]. It can be seen that the barrier height (ϕ) values decreased by increasing the intensity of illumination. This decrease may be illustrated in the terms of band gap narrowing. Variation of the intensity of light changes the occupancy in conduction and valance bands. Consequently, the occupied levels and the unoccupied ones in valance and conduction bands are near to each other producing a reduction band gap and hence reducing the barrier height.

In general, at low bias voltage, the ln(I)–V characteristics are linear but deviate from linearity at high bias voltage because of the series resistance (R_{se}). So that, at high bias voltage the values of R_{se}, n, and ϕ are calculated from the function of Cheung's as [35]:

$$\frac{dV}{d\ln(I)} = IR_{se} + n\left(\frac{kT}{q}\right) \tag{6}$$

$$H(I) = IR_{se} + n\phi \tag{7}$$

Where

$$H(I) = V - n\left(\frac{kT}{q}\right)\ln\left(\frac{t}{AA^{*}T^{2}}\right) \tag{8}$$

Fig. 8 illustrates the dV/dln(I) versus I for Ag/PVA-Ag-Coumarin/n-Si photodiode under dark and different intensities of illumination, respectively, The values of R_{se} and n are calculated from the slope of the linear region and the intercept with y-axis and the results are listed in Table 1. The plot H(I) vs I is depicted in Fig. 9, which denotes a straight line with an intercept of the y-axis (nϕ) and slope denoting the second determination of R_{se}. The values of n, ϕ, R_{se} are recorded in Table 1. By looking again to Table 1. It can be observed that there is a divergence among the barrier height and ideality factor calculated from ln(I)–V in Fig. 7 and dV/dln(I) – I in Fig. 8. This difference may be attributed to the drop in voltage across the depletion layer, the interface states, and series resistance [38].

The interface states distribution can be understood better throughout measuring the effect of illumination intensity upon the diode current. Increasing illumination intensity creates additional free charge carriers that increase the photocurrent. This photocurrent can be inspected through the equation [39]:

$$I_{photo} = \gamma P^{m} \tag{9}$$

where γ is the a constant, P is the illumination intensity and m is an exponent.

Fig. 10 shows the photo-current I_{photo} dependence on light intensity (P). It can be suggested that Ag/PVA-Ag-Coumarin/n-Si is a Schottky

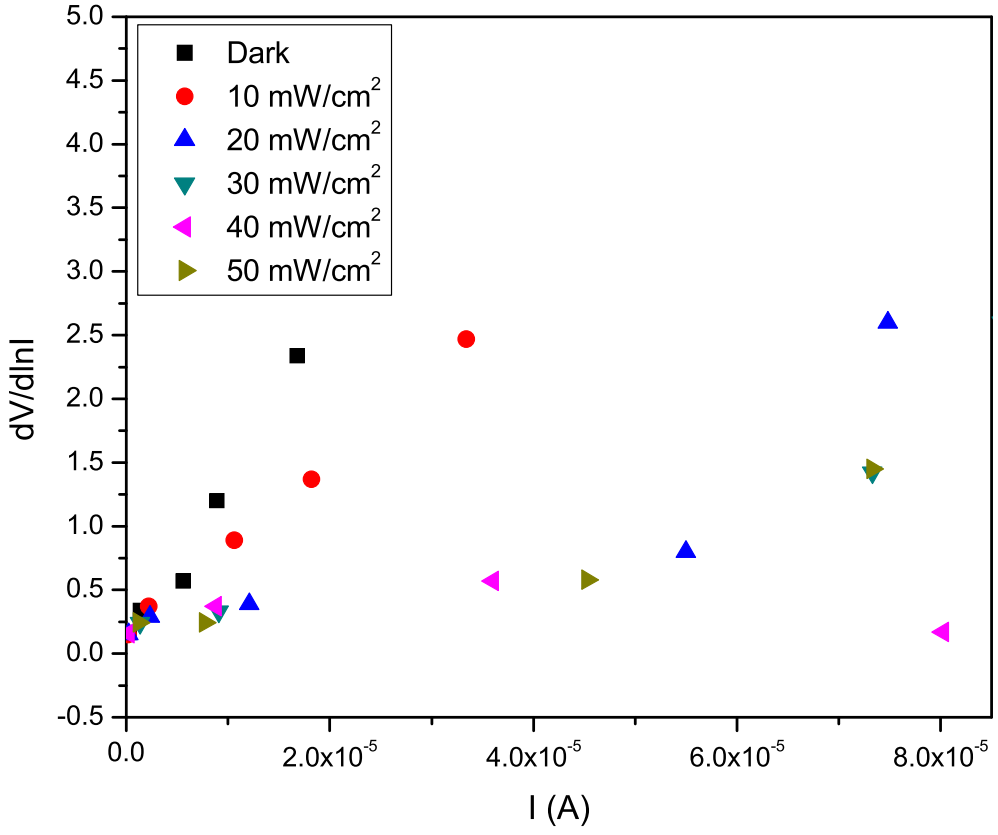

Fig. 8. Shows the dV/dlnI versus I of the Schottky diode under the dark and different intensity of illumination (10–50 mW/cm^2) at room temperature.

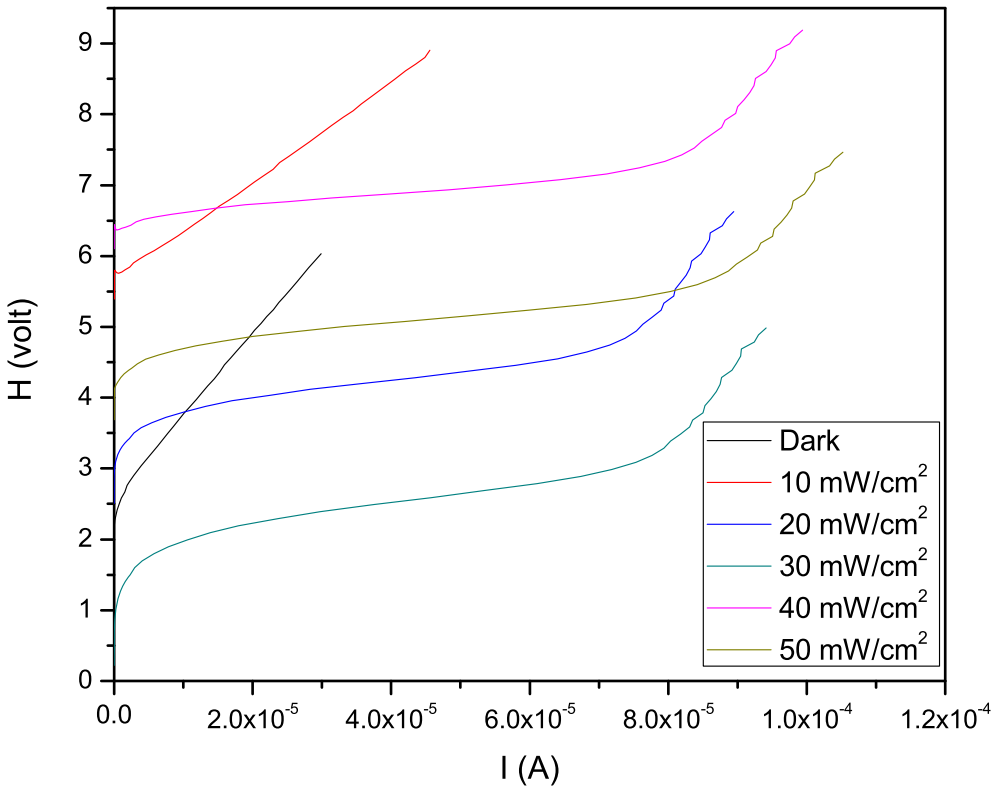

Fig. 9. Shows the H(I) versus I of the Schottky diode under the dark and different intensity of illumination (10–50 mW/cm^2) at room temperature.

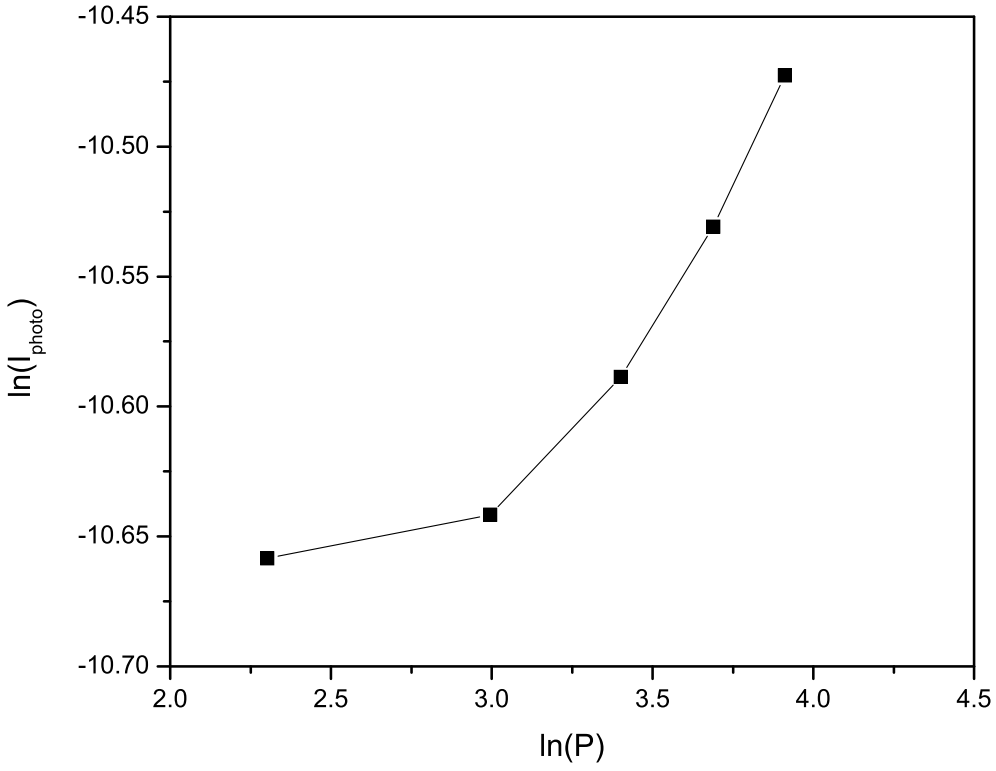

Fig. 10. A plot of ln (I_{Ph}) vs ln (P) of the Ag/PVA -Ag-Coumarin/n-Si Schottky diode.

diode, which could be used as a photosensor. The value of $m = 0.112$ pointed to the presence of localized states that have a regular distribution in the gap of these materials [40].

The time response behavior of the device is clarified in Fig. 11. It can be seen that, I_{photo} grows and reach 160 μA from $I_{Dark} = 20$ μA. The device shows a noticeable sharp change in the current value which means a good and fast response. The response to the light signal was obtained by evaluating the rise time, t_{rise}, and the fall time, t_{fall}. As seen,

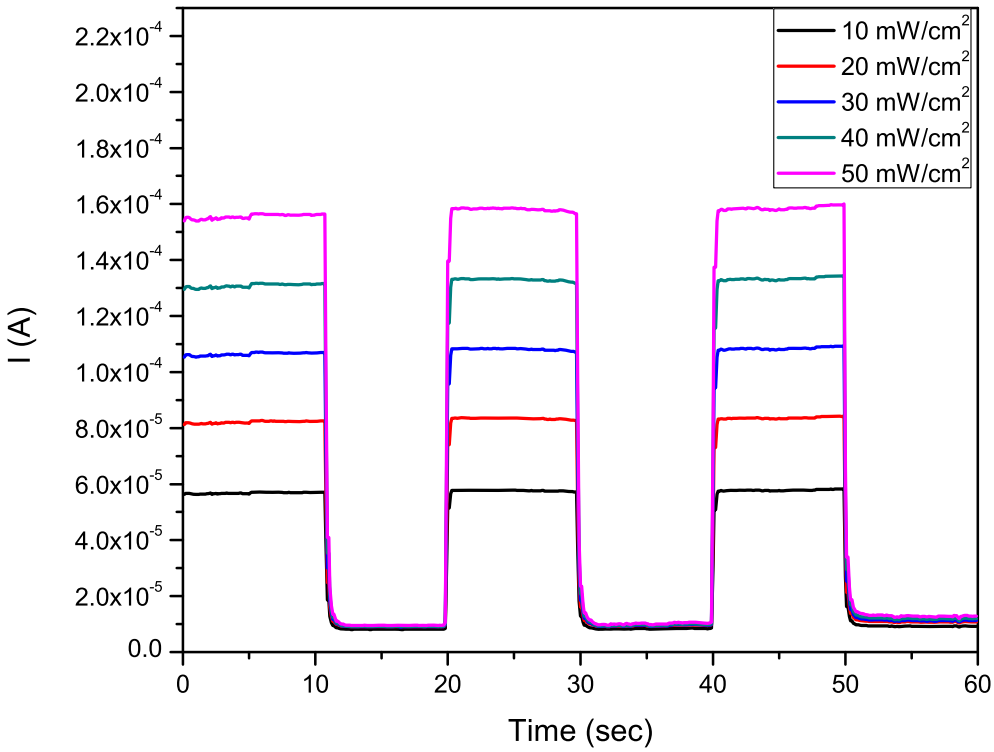

Fig. 11. A Transient photocurrent measurement of Ag/PVA-Ag-Coumarin/n-Si Schottky diode under different intensity of illuminations 10–50 mW/cm.^{2}.

both the rise time and the fall time values decreased from 341 to 90.2 ms, and 482 to 340.6 ms, respectively, just when rising the intensity of light from 10 to 50 mW/cm^2 (Fig. 11). The response time is the time spent for generating excitons, dissociation, and collecting charge carriers as well as the diffusion time of charge and the circuit time constant [41,42]. The excess of (e^-/h^+) pair is the main reason behind the rise and fall time improvement with the growth in the intensity of light. Also, the presence of the interlayer of PVA-Ag-Coumarin composite in the photodiode boosts the silicon absorption on the interface and restricts the charges generated by a photon that is created inside the silicon deep levels which consume a long time for sharing in the generated photocurrent and this explains the slow response to the signals of light [41, 43]. The improvement in our device is clearly observed in Table 2. Table 2 shows the comparison between the diode parameters obtained from our device and the other previous reported devices. In addition to the fast preparation, easy fabrication, affordability, and the simplicity of our structure. Our structure shows a rise time faster than that reported in previous literatures. Also, the ideality factor of our structure (1.463) is lower than the reported literatures giving this structure the opportunity to be a good photodiode. This n value tends to make this structure behave like an ideal photodiode. It can be concluded that the obtained structure in the present work shows higher response than ZnS/InP core/shell NW, ZnS/SnO_2 nanoribbons, PbS QDs/ZnO and $CH_3NH_3PbI_3$/ZnO. The excess of (e^-/h^+) pair is the main reason behind the rise and fall time improvement with the growth in the intensity of light. Also, the presence of the interlayer of PVA-Ag-Coumarin composite in the photodiode boosts the silicon absorption on the interface and restricts the charges generated by a photon that is created inside the silicon deep levels which consume a long time for sharing in the generated photocurrent resulting in the slow response to the signals of light.

Table 2
The comparison between the diode parameters obtained in our diode structure and the other previous reported structures.

Structure	n	t_{rise} (ms)	t_{fall} (ms)	Ref.
Au/PVA-(Co,Zn)/n-Si	1.5	–	–	[44]
ZnS/SnO_2 nanoribbons	–	8×10^3	–	[45]
Al/PVA-10% Coumarin/p-Si	2.3	–	–	[46]
ZnS/InP core/shell NW	–	75×10^1	–	[47]
$CH_3NH_3PbI_3$/ZnO	–	43×10^1	–	[48]
Au/PVA-Bi/n-Si	2.30	–	–	[49]
PbS QDs/ZnO	–	9×10^3	–	[50]
Al/PVA-Bi_2S_3/p-Si	4.48	–	–	[51]
Au/PVA-Co/n-Si	2.5	–	–	[52]
PVA-ZnO/Al	–	22×10^3	–	[53]
Au/PVA-SnO_2/n-Si	4.2	–	–	[54]
Ag/PVA-nGO/p-Si	2.5	–	–	[55]
Al–ZnS NW	–	95×10^3	–	[56]
GaP/ZnS nanocable	–	3×10^2	–	[57]
ZnO–$ZnGa_2O_4$	–	45×10^1	–	[58]
Ag/PVA-Ag-coumarin/n-si	1.463	90.2	340	This work

Capacitance-voltage measurement is common in diode characterization because one can determine the barrier height, built-in potential, the donor in n-type, or the uncompensated ionized density of acceptor in p-type. But the calculated barrier heights through this approach are looked unlike those calculated from the I–V approach. Indeed, the capacitance of diode is a set of depletion and diffusion layer capacitances. Diffusion capacitance ($C_{diffussion}$) and the voltage (V) have a linear relation [59]:

$$C_{diffussion} = \frac{q^2 n_c^2 L_e}{kTN_a} \exp\frac{qc\beta V}{kT} \tag{10}$$

Where q is the electronic charge, n_c is the intrinsic charge carrier concentration, L_e is the excess minority carrier diffusion length, k is constant of Boltzmann, T is the temperature in (kelvin), N_a is the acceptor charge carrier concentration, and c and β are constants. The capacitance of the depletion layer ($C_{diffussion}$) can be possibly described as [60].

$$\frac{1}{C_{depletion}^2} = \frac{2}{q\varepsilon_e A^2 N_{ia}}(V_{bi} + V_{ra} - V_{th}) \tag{11}$$

where $\varepsilon_e = \varepsilon_s\varepsilon_o$ is the permittivity, A is the area of the diode, the built-in voltage is donated by V_{bi}, the non-compensated ionized acceptor density

is donated by N_{ia}, the reverse applied voltage is donated by V_{ra} and V_{th} is the thermal voltage. Fig. 12 shows $(1/C^2_{depletion})$ versus V_{ra} at ambient temperature. From the slope and the intercept, both N_{ia} and V_{bi} can be calculated [61]. The values of the density of non-compensated ionized acceptor (N_{ia}) and built-in voltage (V_{bi}) are shown in Table 2. It can be seen that both N_{ia} and V_{bi} rise with rising frequency. The barrier height (ϕ_b^c) is described by Ref. [62]:

$$\phi_b^c = V_{bi} + \frac{kT}{q}\left[1 + \ln\frac{N_c}{N_i}\right] \quad (12)$$

where N_c is constant. Eq. (12) can be rewritten as:

$$\phi_b^c = V_{bi} + V_{th} + V_p \quad (13)$$

Where

$$V_p = + \frac{kT}{q}\left[\ln\frac{N_c}{N_i}\right] \quad (14)$$

The values of barrier height (ϕ_b^c) as well as the difference in potential between the bottom of the valance band and the Fermi level in the neutral region of the n-silicon (V_p) are shown in Table 3. It can be seen that ϕ_b^c and V_p increase with rising frequency.

Fig. 13. Illustrates the frequency-dependent capacitance-voltage of the Ag/PVA-Ag-Coumarin/n-Si diode. The capacitance behaviour relies on both applied voltage and frequency. It can be depicted that the diode capacitance is reduced by raising the frequency. In the reverse bias region, the capacitance alters clearly with voltage, while in the forward connection, the capacitance slightly varies. The C–V plot clarifies a peak in which its location is shifted together with the applied frequency [63]. This emphasizes the formation of the interface states inside the photodiode. The reduction in the magnitude of the peak with the frequency renders to the existence of a continuous interface state distribution [64]. At the low frequency, the interface states follow up the applied voltage frequency, whereas the interface states at the higher frequencies do not. Therefore, the states of interface do not make any contribution to the capacitance [65].

Table 3
The non-compensated ionized acceptor density (N_{ia}), the built-in voltage (V_{bi}), values of barrier height (ϕ_b^c) and the potential difference between the Fermi level and the bottom of the valance band in the neutral region of the n silicon (V_p).

F (kHz)	$N_{ia} \times 10^{21}$ (m^{-3})	V_{bi} (volt)	ϕ_b^c (volt)	V_p (volt)
5	1.74	14.53	14.74	0.21
10	1.28	18.56	18.78	0.22
20	3.8	53.25	53.45	0.19

4. Conclusion

Schottky (Ag/PVA-Ag-Coumarin/n-Si) diode has been engineered for photodiode applications for the first time. The spin coating technique is applied to fabricate the Schottky device after the preparation of PVA-Ag-Coumarin nano-composite by using the in-situ method. Optical absorption spectra indicate the presence of silver (λ = 436 nm) in the matrix of nano-composite and the results have been confirmed by TEM, SEM and EDX. The effect of coumarin on the absorption spectra was significantly observed especially in the UV region. At ambient temperature, the I–V behavior of the diode displayed an increase in current in both the reverse and forward bias with increasing the intensity of illumination. All the Schottky diode parameters such as n, R_{se}, and ϕ are strong functions of the light intensity. It was observed that the diode has deviated from the ideal behavior, and this may be illustrated on the series resistance basis. Furthermore, the diode shows a high sensitivity to illumination intensities according to I–V characteristics. The experimental results have confirmed that the Ag/PVA-Ag-Coumarin/n-Si device is a good photosensor with superior electrical parameters. The C–V behavior shows that, at a higher positive voltage, the independent behavior of capacitance on both the frequency and voltage can be noticed. Also, in the reverse bias connection, the high capacitance values at lower frequency are ascribed to the surplus capacitance produced from the states of the interface.

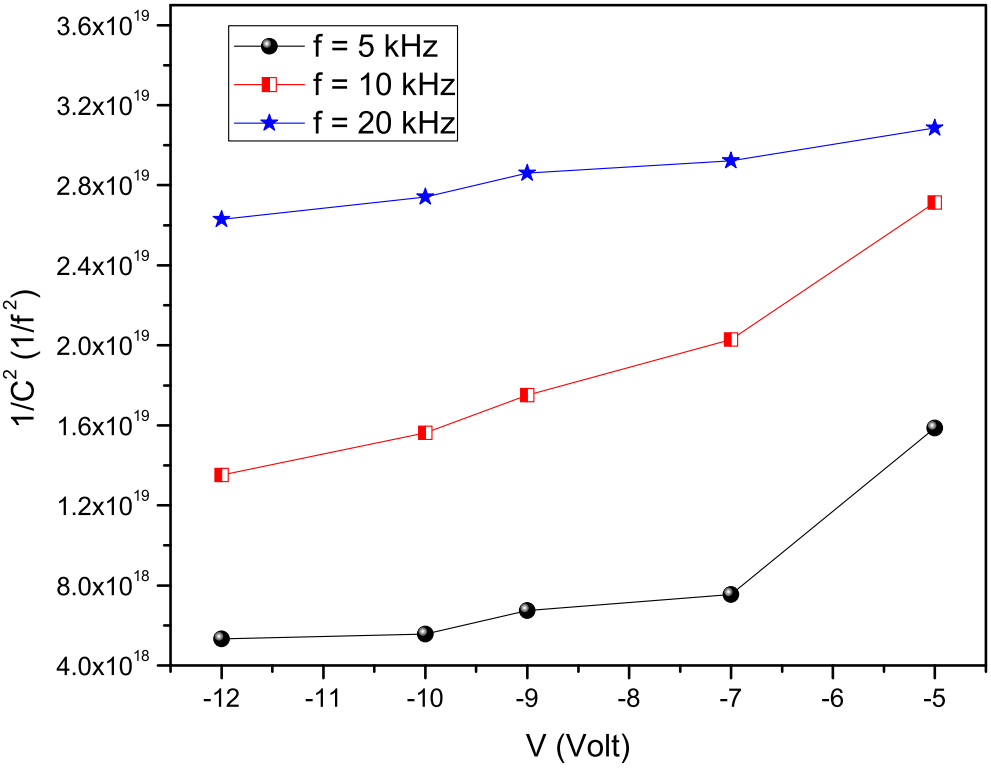

Fig. 12. Shows the relation between $1/C^2$ and V with different frequencies (5, 10 and 20 kHz) at ambient temperature.

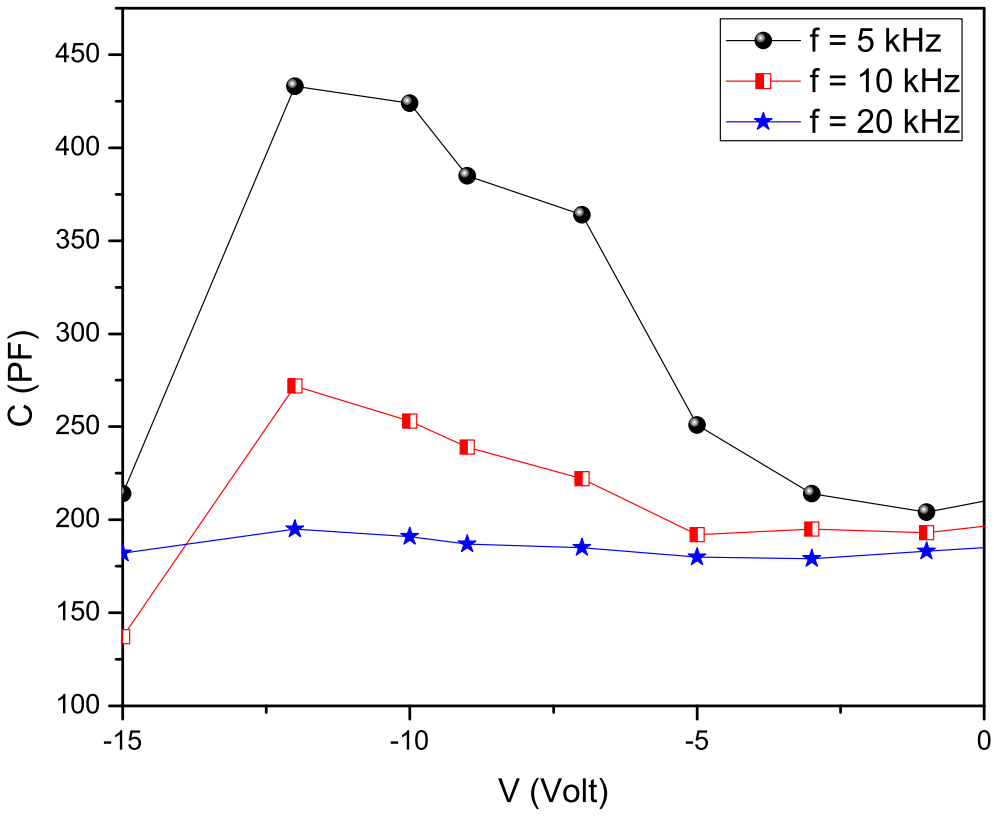

Fig. 13. Frequency-dependent capacitance-voltage (C–V) of Ag/PVA-Ag-Coumarin/n-Si Schottky diode.

CRediT author statement

M.A. Attallah: Methodology, Measurements, Data Curation, Original data, Writing. **T.Y. Elrasasi:** Supervision, Data analysis, Writing. **N. M. Shash:** Supervision, Data analysis, Writing. **M.G. El-Shaarawy:** Supervision, Data analysis, Writing. **F. El-Tantawy:** Supervision, Conceptualization. **Ahmed G. El-Shamy:** Conceptualization, Methodology, Data analysis, Discussion, Writing - reviewing & editing.

Declaration of competing interest

The authors declare that they have no known competing financial interests or personal relationships that could have appeared to influence the work reported in this paper.

References

[1] I. Yun, Photodiodes-from Fundamentals to Applications, InTech, Croatia, 2012.
[2] G.F. Dalla Bett, Advances in Photodiodes, InTech, Croatia, 2011.
[3] Y. Sun, J.A. Rogers, Elsevier, Oxford, 2010.
[4] M. Soylu, I. Yahia, F. Yakuphanoglu, W. Farooq, J. Appl. Phys. 110 (2011), 074514.
[5] A. Farag, I. Yahia, T. Wojtowicz, G. Karczewski, J. Phys. D Appl. Phys. 43 (2010), 215102.
[6] A. Tataroglu, A. Al-Sehemi, M. Ilhan, ·A. Al-Ghamdi, F. Yakuphanoglu, Siliconindia 10 (2018) 913.
[7] M. Saglam, E. Ayyildız, A. Gumus, A. Turut, H. Efeoglu, S. Tuzemen, Appl. Phys. A 62 (1996) 269.
[8] E. Ayyildiz, C. Temiirc, B. Bati, A. Tueruet, Int. J. Electronics 88 (2001) 625.
[9] M. Martin, N. Prasad, M. Sivalingam, D. Sastikumar, B. Karthikeyan, J. Mater. Sci. Mater. Electron. 13 (2017).
[10] A. Hussain, A. Pal, D. Patil, Org. Electron. 15 (2014) 2107.
[11] S. Mousavi, B. Sajad, M. Majlesara, Mater. Des. 162 (2019) 249.
[12] H. Çetinkaya, H. Tecimer, H. Uslu, S. Altındal, Curr. Appl. Phys. 13 (2013) 1150.
[13] A.G. El-Shamy, Prog. Org. Coating 150 (2021), 105981.
[14] A.G. El-Shamy, Mater. Chem. Phys. 257 (2021), 123762.
[15] A.G. El-Shamy, Synth. Met. 267 (2020), 116472.
[16] A.G. El-Shamy, Prog. Org. Coating 146 (2020), 105747.
[17] F. Mir, S. Rehman, K. Asokan, S. Khan, G. Bhat, J. Mater. Sci. Mater. Electron. 25 (2014) 1258.
[18] C. Tang, S. VanSlyke, C. Chen, J. Appl. Phys. 65 (1989) 3610.
[19] A.G. El-Shamy, Polymer 202 (2020), 122565.
[20] A.G. El-Shamy, Mater. Chem. Phys. 243 (2020), 122640.
[21] A.G. El-Shamy, H.S.S. Zayied, Synth. Met. 259 (2020), 116218.
[22] A.G. El-Shamy, W. Attia, K.M. Abd El-Kader, J. Alloys Compd. 590 (2014) 309–312.
[23] A.G. El-Shamy, W. Attia, K.M. Abd El-Kader, Mater. Chem. Phys. 191 (2017) 225–229.
[24] A.G. El-Shamy, A.A. Maati, W. Attia, K.M. Abd El-Kader, J. Alloys Compd. 744 (2018) 701.
[25] D. Phan, R. Gupta, G. Chung, A. Al-Ghamdi, O. Al-Hartomy, F. El-Tantawy, F. Yakuphanoglu, Sol. Energy 86 (2012) 2961.
[26] A.G. El-Shamy, Prog. Org. Coating 127 (2019) 252–259.
[27] A.G. El-Shamy, Mater. Sci. Semicond. Process. 100 (2019) 245–254.
[28] A.G. El-Shamy, Compos. B Eng. 174 (2019), 106993.
[29] A.G. El-Shamy, J. Alloys Compd. 810 (2019), 151940.
[30] January 23rd A.G.A.K. El-Shamy, Polymer/noble metal nanocomposites, nanocomposites - recent evolutions, Subbarayan Sivasankaran, IntechOpen, Available from: https://doi.org/10.5772/intechopen.79016, 2019 https://www.intechopen.com/books/nanocomposites-recent-evolutions/polymer -noble-metal-nanocomposites.
[31] H. Zidan, Polym. Test. 18 (1999) 449.
[32] A.A. Khodiri, M.Y. Al-Ashry, A.G. El-Shamy, J. Alloys Compd. 847 (2020), 156430.
[33] S. Altindal, I. Yucedag, A. Tataroglu, Vacuum 84 (2010) 363.
[34] K. Ejderha, N. Yıldırım, A. Türüt, B. Abay, Superlattice. Microst. 47 (2010) 241.
[35] A. G. El-Shamy, Sensor. Actuator., https://doi.org/10.1016/j.snb.2020.129154.
[36] K. Sasikumar, R. Bharathikannan, M. Raja, Siliconindia 11 (2019) 137.
[37] A. Al-Ghamdi, A. Al-Ghamdi, O. Al-Hartomy, A. Nawar, E. El-Gazzar, F. El-Tantawy, F. Yakuphanoglu, J. Sol. Gel Sci. Technol. 67 (2013) 368.
[38] F. Yakuphanoglu, Sol. Energy 85 (2011) 2518.
[39] M. Reddy, P. Puneetha, Y. Lee, S. Jeong, C. Park, Electron. Mater. 13 (2017) 9.
[40] A. Al-Ghamdi, A. Farag, A. Hendi, R. AlOrainy, Farid El-Tantawy, F. Yakuphanoglu, Appl. Phys. A 121 (2015) 29.
[41] H.G. Çetinkaya, H. Tecimer, H. Uslu, Ş. Altındal, Curr. Appl. Phys. 13 (2013) 1150–1156.
[42] S. Demirezen, Ş. Altındal, I. Uslu, Curr. Appl. Phys. 13 (2013) 53e59.
[43] D. Yang, D. Ma, Adv. Optical Mater. 7 (2019), 1800522.
[44] İ. Dökme, T. Tunç, İ. Uslu, Ş. Altındal, Synth. Met. 161 (2011) 474–480.
[45] X. Huang, Y.Q. Yu, J. Xia, H. Fan, L. Wang, M.G. Willinger, X.P. Yang, Y. Jiang, T. R. Zhang, X.M. Meng, Nanoscale 7 (2015) 5311–5319.
[46] S. Demirezen, S.A. Yerişkin, Polym. Bull. 77 (2020) 49–71.

[47] K. Zhang, J. Ding, Z. Lou, R. Chai, M. Zhong, G. Shen, Nanoscale 9 (2017) 15416–15422.
[48] T. Gao, Q. Zhang, J. Chen, X. Xiong, T. Zhai, Adv. Optical Mater. 5 (2017), 1700206.
[49] S. Alialy, H. Tecimer, H. Uslu, Ş. Altındal, Nanomed. Nanotechnol. 4 (2013) 1000167–1000173.
[50] Z. Zheng, L. Gan, J. Zhang, F. Zhuge, T. Zhai, Adv. Sci. 4 (2017) 1600316.
[51] S. Boughdachi, Y. Badali, Y. Azizian-Kalandaragh, Ş. Altindal, J. Electron. Mater. 47 (2018) 6946–6953.
[52] M. Gökçen, T. Tunç, Ş. Altındal, İ. Uslu, Mater. Sci. Eng. B 177 (2012) 416–420.
[53] S. Sawyer, L. Qin, C. Shing, Int. J. High Speed Electron. Syst. 20 (2011) 183–194.
[54] Ç. Bilkan, Y. Badali, S. Fotouhi-Shablou, Y. Azizian-Kalandaragh, Ş. Altındal, Appl. Phys. A 123 (2017) 560–569.
[55] Ş. Karataş, J. Sandw. Struct. Mater. (2019) 1–21, https://doi.org/10.1177/1099636219840605.
[56] P. Jiang, J.S. Jie, Y.Q. Yu, Z. Wang, C. Xie, X.W. Zhang, C.Y. Wu, L. Wang, Z.F. Zhu, L.B. Luo, J. Mater. Chem. 22 (2012) 6856–6861.
[57] L. Hu, M. Brewster, X. Xu, C. Tang, S. Gradecak, X. Fang, Nano Lett. 13 (2013) 1941–1947.
[58] M. Shahid, J. Cheng, T. Li, M. Ajmal Khan, Y. Wang, Y. Hu, M. Zhang, J. Yang, H. Sartaj Aziz, C. Wan, H. Nishijimac, W. Pan, J. Mater. Chem. C. 6 (2018) 6510–6519.
[59] A. Tataroglu, F. zen, K. Koran, A. Dere, A. Gorgulu, N. Al-Senany, A. Al-Ghamdi, W. Farooq, F. Yakuphanoglu, Siliconindia 10 (2018) 683.
[60] S.M. Sze, K.K. Ng, Physics of Semiconductor Devices, vol. 121, John Wiley& Sons, 1978.
[61] A. Dahlan, A. Tataroglu, A. Al-Ghamdi, A. Al-Ghamdi, S. Bin-Omran, Y. Al-Turki, F. El-Tantawy, F. Yakuphanoglu, J. Alloys Compd. 646 (2015) 1151.
[62] A.N. Donald, Semiconductor physics and devices, in: C.W. Wilmsen (Ed.), Physics and Chemistry of III–V Compound Semiconductor Interface, Plenum, NewYork, 1992, p. 1985.
[63] M. Cavas, M. Aydin, A. Al-Ghamdi, O. Al-Hartomy, F. El-Tantawy, F. Yauphanoglu, J. Opto. electronics and advance. mater 14 (2012) 798.
[64] A. Tataroglu, A. Al-Ghamdi, S. Omran, W. Farooq, F. El-Tantawy, F. Yakuphanoglu, J. Sol. Gel Sci. Technol. 71 (2014) 421.
[65] S. Wageh, A. Al-Ghamdi, Y. Al-Turki, A. Dere, S. Tjong, F. El-Tantawy, F. Yakuphanoglu, Opt. Quant. Electron. 47 (2015) 17798.